Title: Evaluating the Seismic Stability and Performance of Freestanding Geofoam Embankment

Authors: Steven F. Bartlett (Contact Person and Presenter)
Dept. of Civil and Environmental Engineering
122 S. Central Campus Dr.
Salt Lake City, UT 84112
Phone: (801)587-7726
Fax: (801)585-5477
E-Mail: bartlett@civil.utah.edu

Evert C. Lawton
Dept. of Civil and Environmental Engineering
122 S. Central Campus Dr.
Salt Lake City, UT 84112
Phone: (801)585-3947
Fax: (801)585-5477
E-Mail: Lawton@civil.utah.edu

Evaluating the Seismic Stability and Performance of Freestanding Geofoam Embankment

Steven F. Bartlett[1], and Evert C. Lawton[2]

ABSTRACT

The Utah Department of Transportation has made extensive use of expanded polystyrene (EPS) geofoam embankment at select locations on the I-15 Reconstruction Project in Salt Lake City, Utah. This paper presents a method to evaluate the seismic response and stability of a geofoam embankment for a nearby M7.0 earthquake. The recommended approach uses a finite difference numerical model implemented in FLAC (Fast Lagrangian Analysis of Continua) to evaluate the dynamic and deformation response of the geofoam embankment undergoing interlayer sliding and horizontal sway with rocking. The evaluations were performed in a coupled fashion using both the horizontal and vertical components of strong motion of a representative set of acceleration time histories for a nearby M7.0 earthquake. The analyses indicate that interlayer sliding is initiated in some cases and the amount of interlayer sliding displacement depends on the characteristics of the long-period strong motion and the interface properties used in the model. Shear keys strategically placed within the embankment are recommended where the estimated sliding displacements are potentially damaging. The numerical model also suggests that internal deformation caused by rocking and sway can cause local tensile yielding of some blocks within the embankment, usually near the base. In some cases, this yielding can propagate upward and cause the embankment to begin to decouple dynamically. Consideration should be given to using blocks with higher strengths than Type VIII geofoam in the basal zones of geofoam embankments undergoing high levels of strong motion.

[1] Steven F. Bartlett, Dept. of Civil and Environmental Engineering, 122 S. Central Campus Dr.,Salt Lake City, UT, 84112

[2] Evert C. Lawton,Dept. of Civil and Environmental Engineering, 122 S. Central Campus Dr., Salt Lake City, UT 84112

INTRODUCTION

Expanded polystyrene (EPS), commonly known as geofoam, has been increasingly used in the United States as a lightweight embankment material. The single largest application of geofoam in the U.S. was the I-15 Reconstruction Project in Salt Lake City, Utah. During a 3.5-year construction period, the design-build contractor reconstructed approximately 26 km of urban interstate using rapid construction techniques (Farnsworth et al. 2008). Embankment constructed with geofoam played an important role in completing the project within the targeted schedule before the start of the 2002 Olympic Games. Approximately 100,000 m^3 of geofoam block was placed at several bridge approaches and other locales. The primary use of geofoam was to minimize settlement of buried utilities beneath embankments and of nearby buildings and facilities; however, in a few instances it was used to expedite the construction schedule (Bartlett et al., 2000; Farnsworth et al. 2008).

This paper evaluates the expected seismic performance of a typical freestanding geofoam embankment used in Utah by means of numerical modeling techniques incorporated in FLAC^{TM} (Fast Lagrangian Analysis of Continua) (Itasca, 2005). Comprehensive seismic design guidance for geofoam embankment has not been fully developed in the U.S., but Horvath (1995), Stark et al. (2002), Raid and Horvath (2004), and Kalinski and Pentapati (2006) give summaries of pseudostatic and numerical modeling approaches that may be applicable to the seismic design and evaluation of geofoam embankments for specific applications.

At high levels of strong motion, the dynamic response of geofoam embankment is relatively complex. Raid and Horvath (2004) have classified the rigid-body displacement and flexible deformation behaviors present in the geofoam mass as: (1) horizontal flexibility (lateral sway), (2) rigid-body translation (sliding) and (3) rigid-body rotation (rocking). This paper presents a 2D evaluation approach to explore these behaviors and their impact on seismic stability using a representative set of acceleration time histories appropriate for western U.S. near-field earthquakes. This evaluation includes both the horizontal and vertical acceleration components of the candidate time histories in a fully coupled manner.

SEISIMC DESIGN AND INPUTS

For the I-15 Reconstruction Project, the Utah Department of Transportation (UDOT) required that lightweight fill and geofoam embankment placed behind retaining walls be designed to a 500-year return period design basis event (500-yr DBE). Force-based pseudostatic techniques described in Horvath (1995) were used that in short consisted of: (1) calculating the fundamental period of the geofoam embankment, (2) determining the horizontal spectral acceleration for the 500-yr DBE at the fundamental period of the system, (3) calculating the inertial force acting on the centroid of the system as the mass times the spectral acceleration, and (4) using this inertial force in the subsequent stability analyses. The analyses performed by the design-build contractor showed that the geofoam embankment had adequate factors of safety against failure for the 500-yr DBE.

More recently, UDOT has adopted a larger DBE for embankments at bridge approaches. This standard requires that interstate bridges and their approach fills be capable of withstanding a 2500-yr DBE with minimal to no damage. For the Salt Lake Valley, the 2500-yr DBE is characteristically a M7.0 to 7.5 earthquake, that ruptures on the Salt Lake City segment of the Wasatch fault with an expected horizontal PGA of about 0.5 to 0.6 g throughout much of the central part of the Salt Lake Valley. The horizontal and vertical acceleration time histories and their respective response spectra that were used in the evaluations are shown in Figures 1 and 2, respectively and Tables I and II, respectively. These strong motion records were selected from the Pacific Earthquake Engineering Research (PEER) Center website and are unmodified.

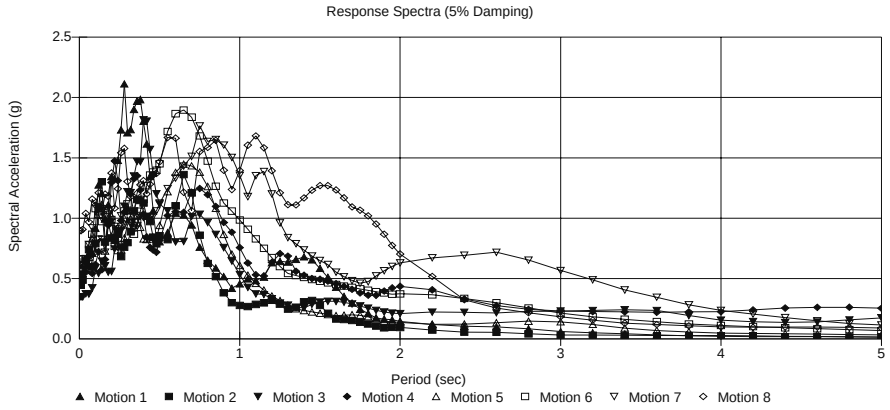

Figure 1. Five percent damped horizontal acceleration response spectra for the evaluation time histories.

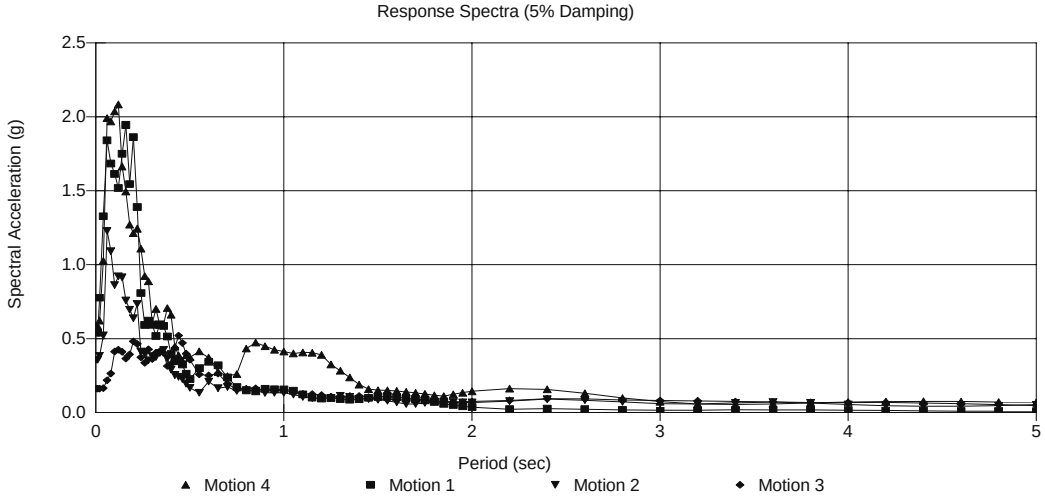

Figure 2. Five percent damped vertical acceleration response spectra for the evaluation time histories.

TABLE I. HORIZONTAL STRONG MOTION RECORDS SELECTED FOR EVALUATIONS.

Motion	Earthquake	M	R (km)	Component	PGA (g)
1	1989 Loma Prieta, CA	6.9	8.6	Capitola 000	0.52
2	1989 Loma Prieta, CA	6.9	8.6	Capitola 090	0.44
3	1999 Duzce, Turkey	7.1	8.2	Duzce 180	0.35
4	1999 Duzce, Turkey	7.1	8.2	Duzce 270	0.54
5	1992 Cape Mendocino, CA	7.1	9.5	Petrolia 000	0.59
6	1992 Cape Mendocino, CA	7.1	9.5	Petrolia 090	0.66
7	1994 Northridge, CA	6.7	6.2	Sylmar 052	0.61
8	1994 Northridge, CA	6.7	6.2	Sylmar 142	0.90

TABLE II. VERTICAL STRONG MOTION RECORDS SELECTED FOR EVALUATIONS.

Motion	Earthquake	M	R (km)	Component	PGA (g)
1	1989 Loma Prieta, CA	6.9	8.6	Capitola up	0.54
2	1999 Duzce, Turkey	7.1	8.2	Duzce up	0.36
3	1992 Cape Mendocino, CA	7.1	9.1	Petrolia up	0.16
4	1994 Northridge, CA	6.7	6.2	Sylmar up	0.59

The acceleration records in Table I and II were selected because their earthquake magnitude, source distance, and soil conditions are similar to those expected for the urban interstate corridor found in the central part of the Salt Lake Valley.

These strong motion records were deconvolved to a depth equal to the base of the 2D numerical model (10 m below ground surface) using the 1D equivalent linear procedures described by Mejia and Dawson (2006). The steps and boundary conditions required to convolve the motion upward through the 2D model are described later.

MODEL DEVEOPMENT AND PROPERTIES

Figure 3 shows a typical freestanding geofoam embankment. At this location, the embankment is approximately 8 m high and 20 m wide and both sides are vertical (i.e., freestanding). The adjacent bridge is supported by piles and the approach slab and adjacent embankment are supported by geofoam. (The geomembrane draped over the geofoam in Figure 3 was removed and not used in the final construction because of concerns of the potential for sliding between the geofoam and geomembrane during a seismic event.) Instead, the load distribution slab was poured directly atop the uppermost geofoam layer.

Figure 4 is a cross-sectional view of a typical geofoam freestanding embankment. From bottom to top, it consists of bedding sand, geofoam block, reinforced concrete load distribution slab, road base (untreated base course), and unreinforced concrete pavement. A prefabricated tilt-up concrete panel wall protects the geofoam from damage and the wall is founded on an embedded slot footing. The panel wall is rigidly connected to the load distribution slab and a coping formed in the concrete pavement protects the panel top (Figure 4). An elastomeric material is placed between the coping and the panel top to limit the vertical and horizontal interaction at this point. In addition, the geofoam blocks do not contact against the back of the panel wall. Typically, a 0.2-m gap is left between the geofoam and the back of the wall to prevent interaction. However, continuous horizontal layers exist in the geofoam mass, which can allow for interlayer sliding if horizontal seismic forces are sufficient to initiate it. No such continuous vertical planes exist, because the blocks are staggered and the orientation is rotated 90 degrees on each successive layer (Figure 4). Lastly, the basal layer (layer 1) of geofoam is placed directly against the slot footing of the tilt-up panel wall and is constrained from horizontal movement.

Because most of the mass of the system is contained within the load distribution slab, road base, and pavement, the geofoam system is often modeled as an elastic single degree of freedom (SDOF) system with the a lumped rigid mass placed at the top and supported by a weightless rectangular geofoam embankment (Horvath, 1995). The combined weight of the load distribution slab, road base and pavement are represented in the lumped mass.

This paper varies from this classic approach in the following important aspects: (1) two degrees of freedom (horizontal and vertical) movement are allowed, (2) nonlinear stress-strain relations are used for all materials, except for the lump mass, which was treated as an elastic material, (3) horizontal sliding is allowed between the geofoam layers by including interfaces nodes, and (4) both the horizontal and vertical components of the strong motion records were inputted into the model to explore their combined effects on the dynamic response and potential sliding.

Figure 3. Typical freestanding geofoam embankment at a bridge abutment.

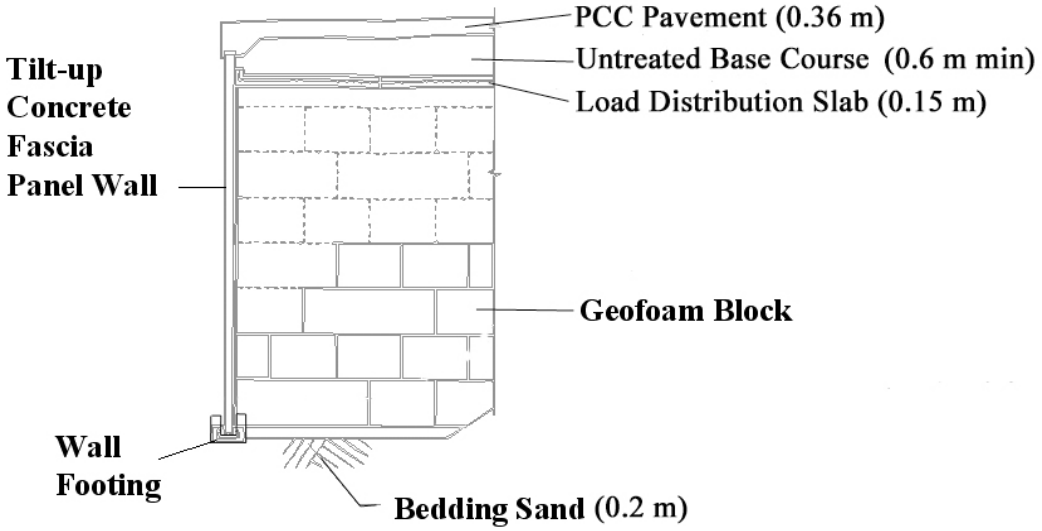

Figure 4. Typical geofoam cross-section used for the I-15 Reconstruction Project.

We chose to model the geofoam embankment using an explicit finite difference program called *FLAC*^{TM} (Fast Lagrangian Analysis of Continua) (Itasca, 2005). The numerical approach, as implemented in *FLAC*, can reasonably approximate the measured pressure distribution and vertical deformation in the geofoam mass for the static load case (Newman et al., in review). *FLAC* also has the capability to model

the 2D nonlinear dynamic response and the potential for interlayer sliding, which is the primary focus of this paper.

The geofoam elastic properties used in the *FLAC* model (Table III) are from large block testing performed by Elragi (2000) and are considered to be representative of the geofoam commonly used on UDOT projects. The various other properties in this table are typical values and their selection, except for the foundation soil, do not affect the modeling greatly. The elastic properties for the foundation soil are representative of a medium to medium-stiff clay, typical for the Salt Lake Valley.

FLAC's hysteretic damping option was used to model the nonlinear strain-dependent modulus and damping in the geofoam and foundation soil. The hysteretic damping option allows the nonlinear formulation in *FLAC* to use the same shear modulus degradation and damping curves developed for the equivalent linear method. Furthermore, the hysteretic damping option eliminates the need for large amounts of Rayleigh damping in the model, which greatly improves *FLAC's* computational speed. The hysteretic damping option can be used with either elastic or Mohr-Coulomb material properties. In the case of the former, nonlinear strain-dependent moduli and damping are calculated, but failure (yielding) does not occur; whereas in the latter case, yielding and plastic behavior are allowed. Because yielding is a form of energy dissipation (damping), for our sliding evaluations we chose to use the elastic properties shown in Table III with hysteretic damping for the geofoam and foundation soil, instead of applying Mohr-Coulomb properties. This essentially means that the geofoam block will not be allowed to yield during sliding, which will in turn emphasize any potential sliding behavior.

Shear modulus degradation and damping curves appropriate for geofoam and the foundation soil were obtained from Athanasopoulos et al. (1999) and Sun et al. (1988), respectively. To implement the hysteretic damping option, *FLAC* offers various functions to fit the curvature of the shear modulus and damping curves. We selected the three-parameter sigmoidal model (sig3) (Itasca, 2005) to fit the shear modulus degradation curves (Figure 5). The sigmoidal model parameters used to obtain these curves are: $a = 1$, $b = -0.45$, and $x_0 = 0.3$ for geofoam and $a = 1.017$, $b = -0.587$, and $x_0 = -0.633$ for the foundation clay.

In addition to hysteretic damping, five percent Rayleigh damping was applied to the *FLAC* model at 200 Hz to eliminate some high frequency artificial numeric vibration that was occurring in the model. Because this damping was only applied to very high frequencies, it has no significant influence on the geofoam and foundation soil response.

We chose a 1 m by 1 m grid spacing for the model that consists of a 10-m thick clay foundation layer, 8-m high geofoam embankment, and 1-m thick lumped mass (Figure 6). The 0.2-m thick bedding sand layer was ignored. In addition, the lumped mass represents the combined masses of the load distribution slab, road base, and concrete pavement. The lumped mass was given elastic properties appropriate for concrete (layer 19, Table III), thus it essentially acts as a coherent system placed atop the geofoam, and because of its high stiffness, will essentially undergo no significant internal deformation.

For simplicity's sake, the panel wall was omitted from the *FLAC* model. Because a gap of 0.2 m is typically used between the geofoam face and the back of the panel wall, the wall does not restrain the geofoam in any manner. However, because the load distribution slab is connected to the panel wall and the load distribution slab interacts with the geofoam along their common contact surface (Figure 4),

TABLE III. INITIAL ELASTIC MODULI AND PROPERTIES FOR THE FLAC MODEL

Material Type	Layer No.	ρ (kg/m^3)[4]	E (MPa)[5]	ν[6]	K (MPa)[7]	G (MPa)[8]
Foundation Soil	1-10	1840	174	0.4	290.0	62.1
Geofoam	11-18	18	10	0.103	4.2	4.5
UTBC[1]	19	2241	570	0.35	633.3	211.1
LDS[2] & PCCP[3]	19	2401	30000	0.18	15625.0	12711.9

[1] Untreated base course, [2] Load distribution slab, [3] Portland concrete cement pavement, [4] Mass density, [5] Initial Young's modulus, [6] Poisson's ratio, [7] Bulk modulus, [8] Shear modulus

some amount of wall/geofoam interaction is expected. This interaction is omitted owing to the extra difficulty in including the wall in the dynamic analyses. Nonetheless, because the mass of the lump mass atop the geofoam embankment is much greater than that of the panel wall, we believe that the FLAC model will capture the primary dynamic behavior of the system.

Interfacial nodes were used at interfaces 1 through 9 to allow sliding and separation in the model between the geofoam layers (Figure 6). Interface 1 is the foundation soil/geofoam contact surface, interfaces 2 through 8 are geofoam/geofoam contact surfaces (from bottom to top, respectively), and interface 9 is a geofoam/load distribution slab contact surface. FLAC requires Mohr-Coulomb properties and normal and shear stiffness at all interfaces. The required properties include: friction, cohesion, tensile strength, normal stiffness, and shear stiffness. However, we applied no cohesion, dilation, or tensile bond strengths at these interfaces. (The lack of tensile bond strength allows for separation between the geoform layers.) Thus, sliding friction was used at the interfaces (Table IV). The friction angles in Table IV were obtained from project-specific laboratory testing performed for the I-15 Reconstruction Project (Bartlett et al., 2000) and represent typical values for Type VIII geofoam. Frictional values for other projects may be somewhat different, depending on material, construction and environmental variables (Bartlett et al. 2000).) In addition, these friction angles are intermediate values between the peak and residual friction angle. We also assumed that dilation due to sliding at the interfaces is negligible. In addition, the effects of gripper plates, which are commonly placed between geofoam layers during construction, are not considered a significant source of sliding resistance due to their relatively small size and were neglected in the analyses. Also the interface between the foundation soil and basal geofoam layer was "glued" so that slippage and sliding does not occur. This was done for two reasons: (1) sliding at this interface is constrained horizontally by the foundation of the panel wall (Figure 4), and (2) we wanted to ensure that full seismic forces are transferred to the geofoam embankment. Lastly, only sliding friction was used at interface 9 at the top of geofoam/bottom of lumped mass contact surface. In reality, this interface is more than a frictional contact, because the concrete slab is poured directly on the geofoam and some tensile and shear bonding undoubtedly occurs; this was neglected in our sliding evaluations.

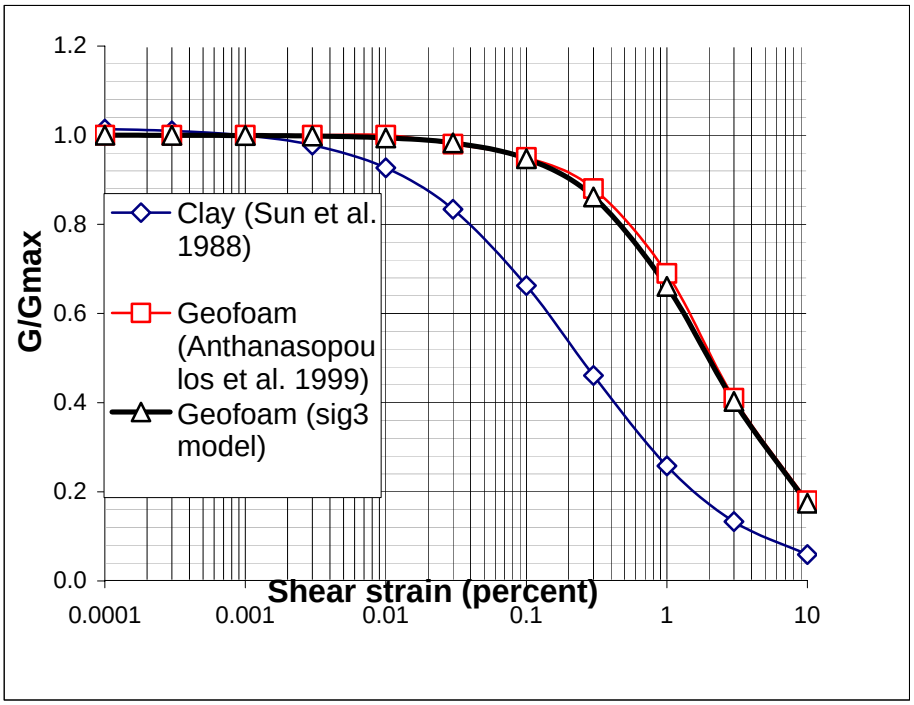

Figure 5. Shear modulus degradation curves used in *FLAC's* hysteretic damping option.

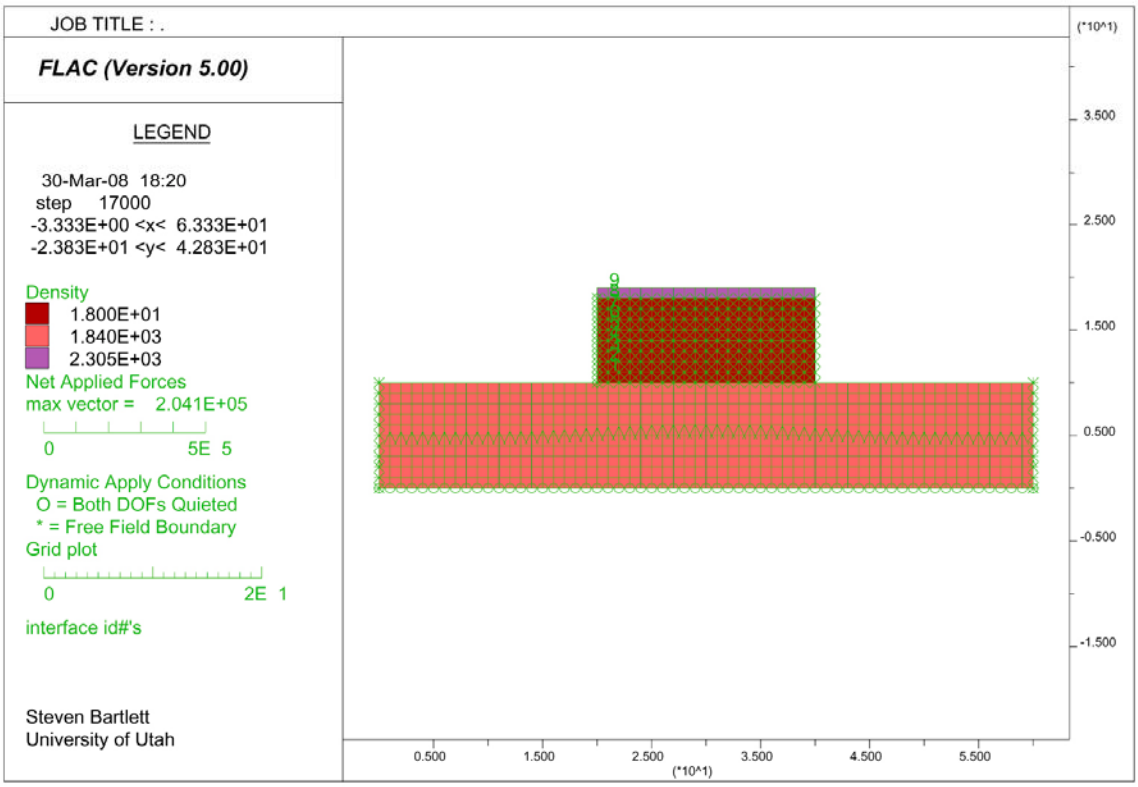

Figure 6. 2D FLAC model used for dynamic and sliding evaluations.

TABLE IV. INTERFACIAL PROPERTIES USED FOR SLIDING EVALUATION IN THE *FLAC* MODEL.

Contact Surface	Interface number (bottom to top)	Normal and Shear Stiffness ($k_n = k_s$) (MPa)	Friction angle (degrees)
Geofoam-soil	1	102	31[1]
Geofoam-Geofoam	2-8	102	38
Geofoam-Lump Mass	9	102	38[2]

[1] *A glued interface was used for interface 1 in FLAC because the geofoam is abutted against the panel wall footing and cannot slide.* [2] *Neglects any tensile or shear bonding that may develop between the top of geofoam and base of the load distribution slab.*

Normal and shear stiffness at the interfaces are also required by *FLAC*. These are spring constants that represent the respective stiffness between two planes that are in contact with each other. Interfacial stiffness is often used in *FLAC* to represent the behavior of rock joints where some elastic deformation in the joint is allowed before slippage occurs. However for geofoam block placed in layers, such elastic behavior before slippage occurs is probably small. Thus, for the case where only slippage and separation are considered at the interface (i.e., one geofoam subgrid is allowed to slide and/or open relative to another subgrid), the normal and shear stiffnesses used in the *FLAC* model are not important (Itasca, 2005). For this case, the *FLAC* user's manual recommends that the normal and shear interface stiffness (k_n and k_s, respectively) be set to ten times the stiffness of the neighboring zone:

$$k_n = k_s = 10\,[(K + 4/3G)/\Delta z_{min}] \quad (1)$$

where: Δz_{min} is the smallest width of an adjoining zone in the normal direction, which is 1 m for our model. However, if the material on one side of the interface is much stiffer than the other, then equation (1) should be applied to the softer side, because the softer side dominates the deformability of the whole system. Thus, making the interfacial stiffness equal to ten times the soft side stiffness ensures that the interface has minimal influence on system compliance (Itasca, 2005). We followed these recommendations for all interfaces.

The final modeling issues to be addressed are the placement of the layers in the model, the applied boundary conditions, and how the strong motion is assigned to the base of the *FLAC* model. First, the *FLAC* model is constructed layer-by-layer and time stepped until force equilibrium is reached in the model. This is done by fixing the base of the model in the x and y coordinate directions and fixing the side of the model, where soil layers are present, in the x direction only. The geofoam is free standing, so no boundary condition is applied along its margins.

When static force equilibrium is reached, the model's boundary conditions are changed for the dynamic case. The bottom of the model is changed to a quiet (i.e., viscous) boundary in both the x and y directions and the sides of the soil model are changed to free-field boundaries (Figure 6). (The free-field boundary forces a 1D free-field boundary condition at the model's edge, which essentially treats the boundary as if it were placed at an infinite distance.) A compliant base is the preferred option for deep soil columns because downward propagating waves are absorbed by the quiet boundary and are not reflected back into the model as would be the case for a rigid boundary (Mejia and Lawson, 2006). The quiet boundary requires a stress time history at the boundary; thus the velocity time history obtained at the base of the soil column from the deconvolution analysis was converted to a stress wave for the subsequent *FLAC* analyses. Itasca (2005) and Mejia and Lawson (2006) provide more information about this conversion and the steps required for deconvolution and convolution analyses. We followed these procedures and to verify the process, the surface acceleration time histories were obtained from *FLAC* at the top of the soil model and were compared with the original input acceleration time histories listed in Tables I and II. This comparison showed that the free-field *FLAC* acceleration time histories were very similar, indicating that the deconvolution/convolution process had been performed correctly and ensuring that the proper level of accelerations were being input to the base of the geofoam embankment.

SUMMARY OF SLIDING EVALUATIONS

The potential for interlayer sliding in a geofoam embankment is often evaluated using pseudostatic techniques. In this approach, the inertial horizontal force at the fundamental period of the geofoam embankment is applied to the sliding calculation. It is calculated by multiplying the lumped mass of the system times the spectral acceleration at the embankment's fundamental period. The geofoam is treated as a SDOF system (Horvath, 1996) and its fundamental period is calculated from Horvath (2004):

$$T_0 = 2\pi\{[(\sigma'_v\, H)/(Eg)[4(H/B)^2 + (12/5)(1+\nu)]\}^{0.5} \quad (2)$$

where: T_0 is the fundamental period, σ'_v is the vertical effective stress acting on the top of the geofoam from dead loads, H is the geofoam embankment height, E is the initial Young's modulus of the geofoam, g is the gravitational constant, B is the width of the geofoam embankment and ν is Poisson's ratio. When applied to the geofoam embankment shown in Figure 6 and the properties given in Table III, the value T_0 is 0.52 s. As a check of the model, the embankment was constructed in *FLAC* on a rigid base and allowed to undergo free-vibration from a pulse load. This produced a T_0 value of 0.51 s, which is good agreement with Equation 2. A pseudostatic sliding calculation applied to our model and interface properties suggests that horizontal accelerations above 0.8 g should trigger sliding. The spectral values at T equals 0.5 s from

Figure 1 vary from about 0.8 to 1.5 g; thus, interlayer sliding is expected to occur for most, if not all, of the input strong motion records.

The *FLAC* model was used to estimate the amount of sliding displacement in the geofoam embankment. To do this, the relative sliding displacement between successive layers of geofoam was calculated and summed as a function of time for all layer interfaces to calculate the total relative sliding displacement (TRSD) time history shown in Figure 7. The maximum TRSD values for each time history case are tabulated in Table V.

The maximum TRSD values range from 0.01 m to greater than 1 m for the various cases listed in Table V. TRSD values less than about 0.1 m are probably acceptable from an embankment performance standpoint; but larger values could have important consequences (i.e., potential damage to the panel wall, damage to approach slabs, etc). The strong motion record used for cases 4a and 4b produced unusually high amounts of sliding (1.3 m). This input horizontal displacement time history is compared with a more moderate sliding case (case 5) in Figure 8, top and bottom, respectively. The Duzce 270 record has a peak horizontal displacement of about 50 cm; whereas the Petrolia 000 record has a much smaller peak horizontal displacement of about 20 cm. This suggests that interlayer sliding is highly affected by the magnitude of the primary displacement pulses, their frequency and phasing.

We noted that TRSD values are usually higher when the vertical component of strong motion is included in the analysis. For example, some cases suggest that sliding displacement increases by a factor of 2 to 5; however, some cases produce essentially the same amount of sliding displacement (Table V). This suggests that the magnitude of the vertical component of strong motion and its relation to horizontal displacement pulses in the horizontal record are important factors that affect sliding. The model also showed that relative sliding is greater near the base of the geofoam embankment and becomes successively less in upper layers (Figure 7). This trend was consistent for all models. No sliding was observed between the top of the geofoam and base of the lumped mass, even though only a friction contact was used at this interface.

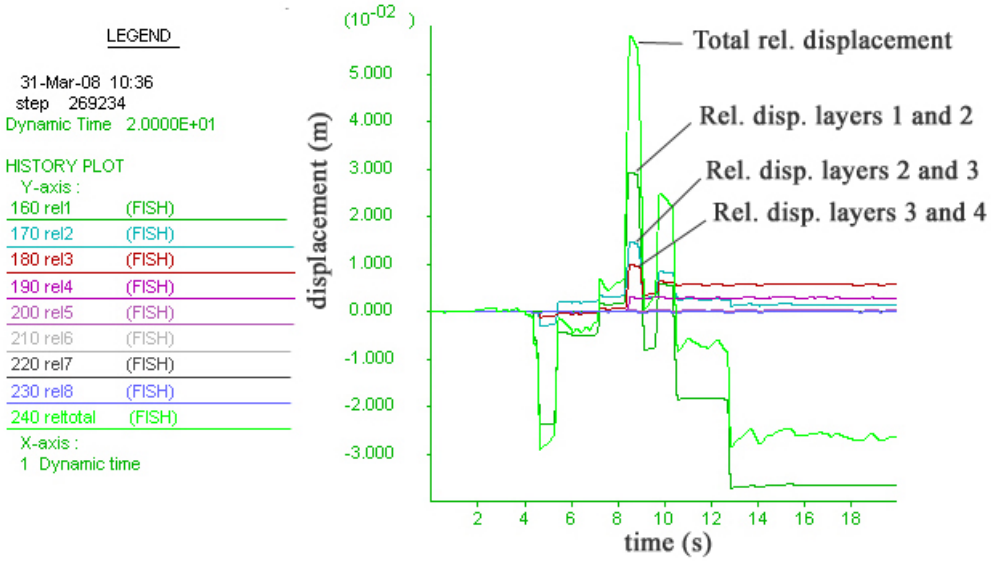

Figure 7. Relative sliding displacement plot for various geofoam layers for case 1a.

Finally, we emphasize that the values reported in Table V are estimates from a numerical model that has not been calibrated with data from case histories or large-scale experiments; thus, some uncertainty exists in these sliding estimates. Because of this, we believe that it is important not to scrutinize solely the estimated displacements, but instead to see if their general magnitudes and trend suggest that a sliding stability threshold has been exceeded where the expected sliding may become unacceptably large. For example, two of the eight cases that included the vertical component of strong motion had TRSD values greater than 0.1 m (cases 4b and 8b). Because this represents 25 percent of the vertical + horizontal component cases, it is probable that sliding displacement may be unacceptable for the particular geofoam configuration and DBE represented in our evaluations.

The potential for interlayer sliding in geofoam embankments can be easily addressed during construction. For large earthquakes, with significant nearby strong motion, we recommend that shear keys be constructed in the geofoam embankment to disrupt any continuous horizontal slide planes created by using current block placement practices. Shear keys are constructed by periodically installing half-height blocks in the geofoam mass that interrupt the horizontal planes. The strategic placement of shear keys will require the potential sliding surface to shear through a select number of geofoam blocks. Because of the relatively high shearing strength of the blocks, this pattern of placement will disrupt the failure surface and greatly improve the sliding resistance.

HORIZONTAL SWAY AND ROCKING

In addition to horizontal translation (i.e., sliding), Raid and Horvath (2004) discuss horizontal sway and rigid body rocking as fundamental free-standing geofoam embankment behaviors. Horizontal sway results from flexibility of the geofoam mass in the horizontal (x) direction, and rocking results from 2D rigid body rotation (Raid and Horvath, 2004).

In reality, the geofoam embankment is flexible when subjected to strong motion and will undergo both horizontal and vertical internal deformation as the mass attempts to sway and rock in response to the earthquake strong motion. Horizontal sway will primarily induce shear stresses and strains; whereas attempted rocking will mainly produce alternating tensile and compressive stresses and their associated strains as the geofoam mass attempts to rock. If the rocking behavior is sufficiently large, then uplift may occur at the basal corners of the geofoam embankment.

The potential consequences of the above behaviors were explored using the developed *FLAC* model with the following modifications to the interfacial, material property, and loading conditions. First, we bonded all of the interfacial nodes within the geofoam mass (interfaces 2 through 9) to limit interface sliding, as if shear keys had been constructed in the mass. *FLAC* allows both tensile and shear bonds as interfacial properties. These values were set equal to the tensile and shearing strength of the geofoam (117.5 and 159 kPa, respectively), which are applicable to Type XIII geofoam (Benchmark Foam, 2003). A bonded interface also allows for a friction angle to be specified, so that when the bond is broken, friction can act along the interface. This value was set equal to 38 degrees (Table IV). Slippage along the interface was not allowed until the bond was broken. Second, a bonded interface condition was also specified at interface 9 (top of geofoam/bottom of lumped mass). The tensile bond at this location was also set equal to 117.5 kPa, which essentially means that the bond between the concrete and geofoam is strong enough that the geofoam will be ruptured in tension according to its tensile capacity before the bond is broken. In addition, a shear bonding of 70 kPa was used at this interface based on concrete/geofoam interface shear test data from Sheeley and Negussey (2000). A friction angle of 38 degrees was also assigned to this interface, which will only be used if the bond breaks. Third, the interface between the geofoam and the foundation soil (interface 1) was unglued, which will allow vertical separation (uplift). Any horizontal sliding displacement at this interface was limited by assigning a very high friction angle (89 degrees), which precluded horizontal sliding. Like the sliding model, this was done to constrain the basal geofoam horizontally, which models the actual horizontal restraint provided by the panel wall footing (Figure 4). However, uplift was still allowed at this interface to allow

for any rocking/uplift behavior. Fourth, the Mohr-Coulomb model with hysteretic damping was applied to all geofoam layers to see if yielding is reached in the block during earthquake cycling. The geofoam was assigned tensile and shearing strengths of 117.5 kPa and 159 kPa, respectively (Benchmark Foam, 2003). Lastly, we only considered cases with both the vertical and horizontal components of strong motion.

TABLE V. SUMMARY OF RELATIVE SLIDING DISPLACEMENT.

Case	Horizontal Motion	Vertical Motion	Max. total relative sliding displacement (m)
1a	1	Not applied	0.06
1b	1	1	0.06
2a	2	Not applied	0.01
2b	2	1	0.05
3a	3	Not applied	0.06
3b	3	2	0.06
4a	4	Not applied	1.3
4b	4	2	1.3
5a	5	Not applied	0.005
5b	5	3	0.01
6a	6	Not applied	0.05
6b	6	3	0.06
7a	7	Not applied	0.5
7b	7	4	0.6
8a	8	Not applied	0.6
8b	8	4	0.5

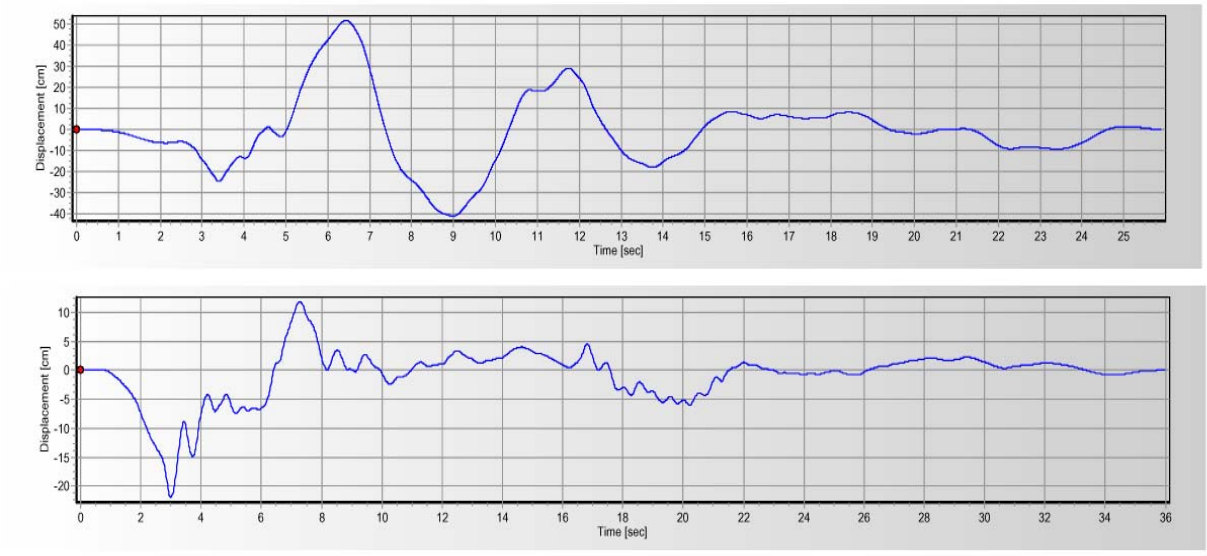

Figure 8. Comparison of Duzce 270 input displacement time history (Case 4) (top) versus Petrolia 000 input displacement time history (Case 5) (bottom).

Table VI summarizes the maximum uplift at the embankment corners and general behavior for the horizontal sway and rocking case. The analyses suggest that some uplift occurs at the corners of the geofoam embankment that ranges from about 0.01 to 0.2 m. Horizontal sway and rocking modes can cause localized tensile yielding of the block that primarily occurs in the basal geofoam layers. However, in two cases, the tensile yielding propagated to higher levels in the embankment, causing the embankment to begin to decouple dynamically (Figure 9). Thus, we recommend that consideration be given to installing higher strength geofoam block (denser than Type VIII geofoam) in the basal layers of geofoam embankments to prevent this behavior. In addition, in a few cases, the interfacial bond between the top of the geofoam and the load distribution slab was broken during the modeling and the lumped mass above the geofoam began to slide atop the geofoam (Figure 9). Design considerations should be given to this contact surface to ensure that sufficient bond strength is available to prevent decoupling. In addition, placement of a geomembrane at this interface, as shown in Figure 3, is not recommended due to the relatively low angle of friction that realized at this contact surface. (Note that this geomembrane shown in Figure 3 was removed prior to pouring the load distribution slab due to sliding concerns at this interface).

CONCLUSIONS

In general, the majority of the evaluated cases suggest that interlayer sliding is within tolerable limits (0.01 to 0.1 m); however, two input time histories produced interlayer sliding that was greater than 0.5 m, which is considered unacceptable from a performance standpoint. Because the model predicted a wide range of interlayer sliding displacement for the cases analyzed, this suggests that sliding is a highly nonlinear process and is strongly governed by the frequency content and long period displacement pulses present in the input time histories.

The model also suggests that interlayer sliding displacement can, in some cases, increase when the vertical component of strong motion is included in the analysis. For cases where interlayer sliding is just initiating, the sliding displacement increases by a factor of 2 to 5 times when the vertical component of strong motion is added to the analyses. However, when the interlayer sliding displacements are larger, the presence of the vertical component in the model is less important and the displacements remain the same or only slightly increase. Thus, we conclude that it is generally unconservative to ignore the vertical component of strong motion when estimating sliding displacement, but its inclusion is less important when the interlayer sliding displacement is well developed. All models showed that the interlayer sliding is generally concentrated in the basal layers and diminishes greatly in the higher layers. The potential for interlayer sliding displacement in geofoam embankments can be resolved by constructing shear keys within the geofoam mass to disrupt continuous horizontal layers that are being created by current construction practices.

The numerical model also suggests that internal deformation caused by rocking and sway can cause local tensile yielding of some blocks within the embankment, usually near the base. In some cases, this yielding can propagate upward and cause the embankment to begin to decouple dynamically. Consideration should be given to using blocks with higher strengths than Type VIII geofoam in the basal zones of geofoam embankments undergoing high levels of strong motion.

TABLE VI. SUMMARY OF HORIZONTAL SWAY AND ROCKING DISPLACEMENT AND BEHAVIOR.

Case	Max. uplift (left corner) (m)	Max. uplift (right corner) (m)	Local Yielding of Block	Bond broken between geofoam and LDS[1]
1b	0.06	0.05	No	No
2b	0.02	0.04	No	No
3b	0.2	0.2	Yes (some blocks in basal layer and 1 block under LDS)	Yes
4b	0.2	? rotation due to tensile yielding	Yes (some blocks in basal layers; tensile yielding developing)	Yes
5b	0.01	0.01	No	No
6b	0.03	0.03	No	No
7b	? rotation due to tensile yielding	0.2	Yes (some blocks in basal layers; tensile yielding developing)	Yes
8b	0.25	0.25	Yes (some blocks in basal layer)	No

[1] LDS = Load distribution slab

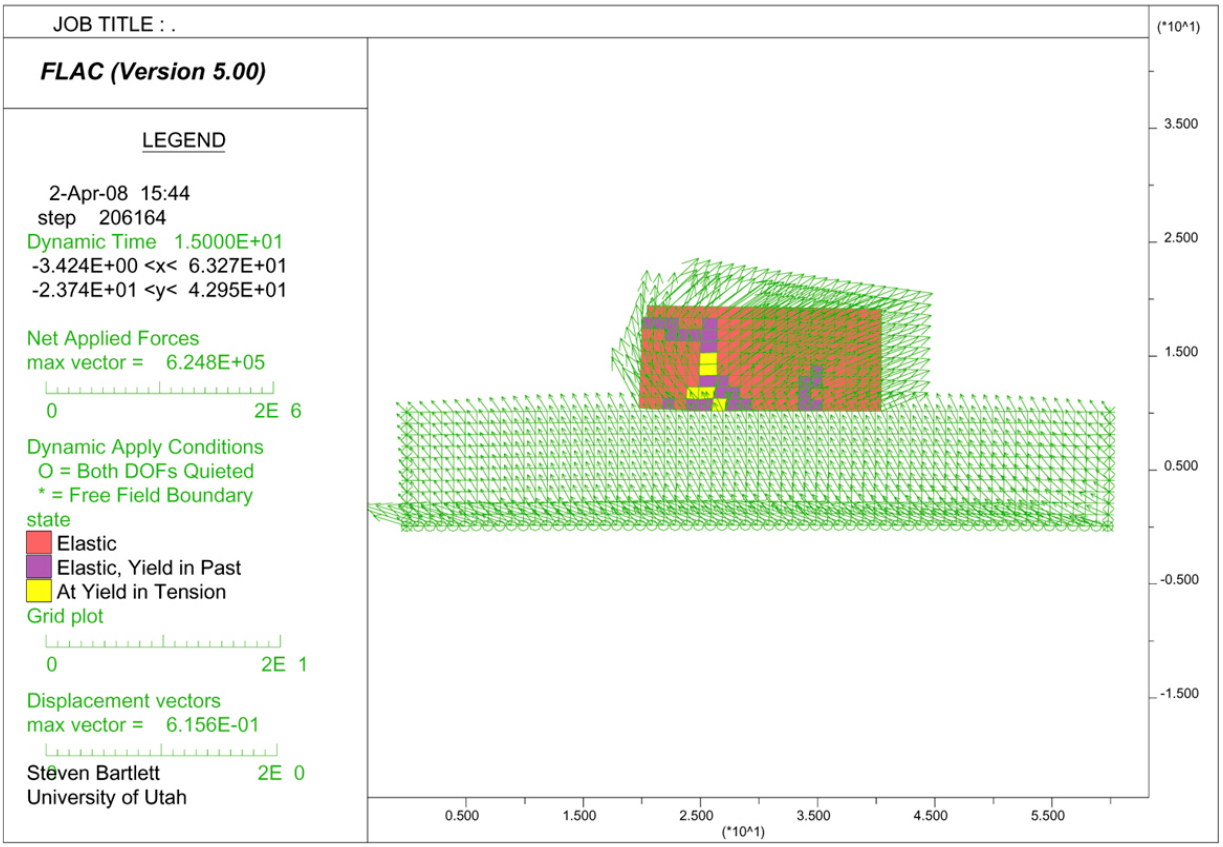

Figure 9. Upward propagation of tensile yielding in the geofoam embankment and decoupling of the load distribution slab for case 7b.

REFERENCES

Anthanasopoulos, G. A., Pelekis, P. C. and Xenaki, V. C. (1999). "Dynamic Properties of EPS Geofoam: An Experimental Investigation," Geosynthetics International, Vol. 6, No. 3.

Bartlett, S., Negussey, D., Kimble, M., and Sheeley, M. (2000). "Use of Geofoam as Super-Lightweight Fill for I-15 Reconstruction." Transportation Research Board 79th Annual Meeting, Washington, D.C.

Benchmark Foam (2003). "Physical Properties of EPS," Benchmark Form Corp., 3200 9th Ave. SE, Watertown, SD 57201.

Elragi, A.F. (2000). "Selected Engineering Properties and Applications of EPS Geofoam." PhD Dissertation. State University of New York College of Environmental Science and Forestry, Syracuse, NY.

Farnsworth C. F., Bartlett S. F., Negussey, D. and Stuedlein A. (2008). "Construction and Post-Construction Settlement Performance of Innovative Embankment Systems, I-15 Reconstruction Project, Salt Lake City, Utah," Journal of Geotechnical and Environmental Engineering, ASCE (Vol. 134 pp. 289-301).

Horvath, J. S. (2004). "A Technical Note Regarding Calculating the Fundamental Period of an EPS-Block-Geofoam Embankment," Report No. CGT-2004-1, Manhattan College, School of Engineering, Center for Geotechnology, 10 p.

Horvath, J. S. (1995). Geofoam Geosynthetic, published by Horvath Engineering, P.C., Scarsdale, New York, U.S.A.

Itasca Consulting Group, Inc. (2005). "*FLAC*: Fast Lagrangian Analysis of Continua: Structural Elements, Version 5." Minneapolis, Minnesota.

Kalinski, M. E. and Pentapati, D. P. (2006). "Numerical Simulation of Dynamic Behavior of Geofoam Embankment," Transportation Research Record, No. 1975, pp. 89-95.

Mejia, L. H. and Dawson, E. H. (2006). "Earthquake Deconvolution in FLAC," 4th International FLAC Symposium in Numerical Modeling in Geomechanics, 2006 Itasca Consulting Group Inc., Minneapolis MN.

Newman, M. P., Bartlett S. F., Lawton, E. C. (in review) "Numerical Modeling of Geofoam Embankments," Journal of Geotechnical and Environmental Engineering, ASCE (in review).

Riad, H. L. and Horvath, J. S. (2004). "Analysis and Design of EPS-Geofoam Embankments for Seismic Design," ASCE Geo-Trans 2004, July 27-31, Los Angeles, California.

Sheeley M. and Negussey D. (2000). "An Investigation of Geofoam Interface Strength Behavior," Proceedings of the Soft Ground Technology Conference, ASCE Geotechnical Special Publication 112.

Stark, T. D., Arellano, D., Horvath, J. S. and Leshchinsky, D. (2002). *Guidelines for geofoam applications in embankment projects*, Final Rpt. - Natl. Coop. Hwy. Res. Prog. Proj. No. 24-11.

Sun, J. I., Golesorkhi, R. and Seed, H. B. (1988). "Dynamic Moduli and Damping Rations for Cohesive Soils," Earthquake Engineering Research Center, University of California, Berkeley, Report No. UCB/EERC-88/15, 42 p., 1988.